Asia-Pacific J. Atmos. Sci., 49(4), 483-496, 2013
DOI:10.1007/s13143-013-0043-9

Sensitivity of Simulated Intraseasonal Oscillation to Four Convective Parameterization Schemes in a Coupled Climate Model

Suryun Ham and Song-You Hong

Department of Atmospheric Sciences, Yonsei University, Seoul, Korea

(Manuscript received 11 October 2012; revised 23 January 2013; accepted 24 January 2013)

Abstract: This paper investigates the sensitivity of a simulated tropical precipitation climatology focusing on the intraseasonal oscillation (ISO) to four convective parameterization schemes: simplified Arakawa-Schubert (SAS), relaxation Arakawa-Schubert (RAS), new Kain-Fritsch (KF2), National Center for Atmospheric Research (NCAR) Climate Model version 3 (CCM). An 8-year boreal summer climatology from 1997 to 2004 is constructed using an ocean-atmosphere coupled global climate model (GCM). The simulated tropical precipitation climatology shows that all four experiments capture the observed climatology fairly well, with the pattern correlation coefficients greater than 0.8. The ensemble mean of results from the four experiments does not reveal a benefit in reproducing the observed precipitation climatology or the ISO signals. Although the KF2 scheme has been most widely tested and updated in mesoscale modeling communities, its capability in tropical climate simulation is shown to be relatively good in terms of sea surface temperature (SST) and precipitation. Results from the SAS and KF2 schemes show similar patterns in terms of climatology and ISO signals, with a greater precipitation variance than that from other experiments. The ISO signals from the RAS run show relatively realistic ISO signals, but with too strong intensity. Our study implies that the appropriate partitioning of deep convection due to cumulus parameterization scheme and stratiform precipitation due to microphysics scheme should be taken into account when developing or revising physics algorithms in coupled GCMs.

Key words: Convective parameterization scheme, tropical climate simulation, intraseasonal oscillation, Madden Julian oscillation

1. Introduction

The tropical intraseasonal oscillation (ISO), known as the Madden Julian oscillation (MJO), is the most important variability at the subseasonal time scale and is the dominant mode in the tropical region, with eastward periods of 30-60 days (Madden and Julian, 1971). It is characterized by eastward-propagating, equatorially trapped, baroclinic oscillations in the tropical wind field. During a typical ISO event, a positive convection/rainfall anomaly develops over the western Indian Ocean, while convection tends to be suppressed further east over the western Pacific. Over the course of the following 40-50 days, the enhanced convective anomaly in the Indian Ocean intensifies and propagates slowly eastward to the central Pacific Ocean. The convection anomalies associated with the ISO are most intense over the central/eastern Indian Ocean and western Pacific Ocean (Kiladis *et al*., 2005; Waliser *et al*., 2009).

Many studies have reported the ISO to have an influence on the character and strength of higher-frequency modes of tropical variability, including the diurnal cycle (Chen *et al*., 1996; Tian *et al*., 2006), tropical cyclones (Bessafi and Wheeler, 2006; Frank and Roundy, 2006), and extreme precipitation events (Mo and Higgins, 1998; Jones, 2000). However, resultant improvements in the simulation of the ISO in general circulation models (GCMs) are considerably limited (Fu *et al*., 2008; Kim *et al*., 2009). Lin *et al*. (2006) demonstrated that only two models out of the 14 coupled GCMs participating in the Intergovernmental Panel on Climate Change (IPCC) Fourth Assessment Report (AR4) were able to simulate MJO variance and the pronounced 30- to 60-day spectral peaks that are consistent with observations.

The inability of models to simulate the ISO has long been thought to be related to deficiencies in the treatment of precipitating convection since most of the tropical precipitation in GCMs is produced by the cumulus parameterization scheme (CPS) algorithm. Several studies compared the capability of CPSs in reproducing the ISO (e.g., Chao and Deng, 1998; Lee *et al*., 2003; Park *et al*., 2010). Chao and Deng (1998) compared the three CPSs in the 3D Aqua-Planet GCM, and found mechanisms in simulating the ISO and super cloud clusters. Lee *et al*. (2003) found that the moist convective adjustment scheme tends to produce intense point-like convective storms, while the mass flux scheme tends to simulate low-intensity drizzling precipitation. Park *et al*. (2010) compared the two Arakawa-Shubert type CPS algorithms in a GCM, and demonstrated a plausible link between the ISO and dynamic seasonal prediction.

Meanwhile, it has also been reported that specific closures would improve the simulation of ISO in specific models but would have an opposite effect in other models. For example, Wang and Schlesinger (1999) showed that a large relative humidity threshold in convective parameterization is critical for the amplification of ISO by causing a time lag between condensational heating and large-scale convergence. On the other hand, the Community Climate Model (CCM) experiments

Corresponding Author: Song-You Hong, Dept. Atmospheric Sciences, College of Science, Yonsei University, 50 Yonsei-ro, Seodaemun-gu, Seoul 120-749, Korea.
E-mail: songyouhong@gmail.com

by Maloney and Hartmann (2001) indicated that the ISO signal of the model is not sensitive to the relative humidity threshold. These studies imply other factors in the simulation of ISO, that is, the model dependency. For example, if a model fails to capture the observed convection-heat flux relationships due to model deficiencies such as the generation of erroneous mean surface wind fields and sea surface temperature (SST), the simulated ISO may not be improved satisfactorily (Sperber *et al*., 2005).

As the interaction between moist convection and the ISO becomes to be understood, some researchers endeavored to improve the cloud microphysics in existing CPSs in order to enhance the predictability of the ISO and mean climate (e.g., Zhang and Mu, 2005; Fu and Wang, 2009; Seo and Wang, 2010). Fu and Wang (2009) found that detrainment from the convective updrafts moistens the large-scale environment and induces the further development of deep convective plumes. They also showed that the convective detrainment of moisture to stratiform clouds plays a key role in sustaining the MJO. Seo and Wang (2010) reported that the convective detrainment of moisture plays a key role in sustaining the ISO by inducing a characteristic heating profile.

In this study, four different CPSs, namely the simplified Arakawa-Schubert (SAS) scheme (Hong and Pan, 1998), relaxation Arakawa-Schubert (RAS) scheme (Moorthi and Suarez, 1992), new Kain-Fritsch (KF2) scheme (Kain, 2004), and National Center for Atmospheric Research (NCAR) Community Climate Model version 3 (CCM) scheme (Zhang and McFarlane, 1995) are evaluated on an ocean-atmosphere coupled testbed with the inclusion of diurnal variation of SST. Our study differs from previous studies that compare the CPSs on an atmospheric GCM (AGCM) only or atmosphere-ocean GCM (AOGCM) framework that couples on a daily basis. The KF2 scheme that has been widely applied in regional modeling communities is evaluated, for the first time, to check its ability to reproduce simulated global climatology in addition to the ISO signals. The coupled model used in this study is a newly developed GCM (Hong *et al*., 2013). Simulations are conducted for boreal summers from 1997 to 2004 with a focus on evaluating the simulated precipitation climatology and associated ISO.

This paper is organized as follows. The details of the model, experiments, and datasets are discussed in section 2. Results regarding the sensitivity of the ISO to different convection schemes in the tropical climate are explained in section 3. Finally, a conclusion is presented in section 4.

2. Experimental design

a. Model description

The global atmosphere-ocean coupled model is a component of the recently developed Global/Regional Integrated Model system (GRIMs) (Hong *et al*., 2013). The GRIMs was created for use in numerical weather prediction, seasonal simulations, and climate research projects on global to regional scales. In addition to the conventional spherical harmonics (SPH) dynamical core for the global model program (GMP), a double Fourier series (DFS, Cheong, 2006) core is included as an alternative. A single-column model (SCM) program was devised for effective evaluation of physics algorithms, and the Aqua-Planet was used to test the interaction of dynamics and physical parameterizations in atmospheric models. The regional model program with the scale selective spectral nudging (Hong and Chang, 2012) has been applied to downscaling of climate changes. The history and configuration of the GRIMs and its capabilities in numerical weather prediction and climate simulations were demonstrated in Hong *et al*. (2013).

The atmospheric component of the model employs a resolution of T62L28 (triangular truncation at wave number 62 in the horizontal and 28 terrain-following sigma layers in the vertical). We employ the GRIMs model physics version 3.1, which includes longwave and shortwave radiation (Chou *et al*., 1999; Chou and Suarez, 1999; Chou and Lee, 2005), planetary boundary-layer processes (Hong *et al*., 2006), shallow convection (Hong *et al*., 2012), gravity-wave drag (Kim and Arakawa, 1995; Chun and Baik, 1998; Jeon *et al*. 2010), simple hydrology, and vertical and horizontal diffusion. For precipitation physics, both stratiform precipitation processes (Hong *et al*., 1998) and the cumulus parameterization schemes are employed.

The ocean component is the Geophysical Fluid Dynamics Laboratory (GFDL) Modular Ocean Model version 3 (MOM3) (Pacanowski and Griffies, 1998), which is a finite difference version of the ocean primitive equations under the assumptions of Boussinesq and hydrostatic approximations. It uses spherical coordinates in the horizontal with a staggered Arakawa B grid and the z coordinate in the vertical. The domain is quasi-global, extending from 74°S to 64°N. The zonal resolution is 1°. The meridional resolution is 1/3° between 10°S and 10°N, gradually increasing through the tropics until becoming fixed at 1° poleward of 30°S and 30°N. There are 40 layers in the vertical with 27 layers in the upper 400 m, and the bottom depth is around 4.5 km. The vertical resolution is 10 m from the surface to a depth of 240 m, gradually increasing to about 511 m in the bottom layer.

The atmospheric and oceanic components are coupled with no flux adjustment or correction. The two components exchange daily averaged quantities, such as heat and momentum fluxes, once a day. Due to the difference in latitudinal domain, full interaction between atmospheric and oceanic components is confined to 65°S to 50°N. Poleward of 74°S and 64°N, the SSTs needed for the atmospheric model are taken from observed climatology. Between 74°S and 65°S and between 64°N and 50°N, SSTs for the atmospheric component are a weighted average of the observed climatology and the SST from the ocean component of the GRIMs.

The diurnal variation of SST considering the wind-driven mixed-layer cooling as well as the surface energy budget over the oceans is represented (Kim and Hong, 2010). The ocean mixed layer (OML) depth is initialized to the global climatology

field of the Naval Research Laboratory OML depth (Kara *et al*., 2003) every 0000 UTC. Kim and Hong (2010) showed that the inclusion of the ocean mixed-layer model cools the water surface due to enhanced mixing using the Weather Research and Forecasting (WRF) model (Skamarock *et al*., 2008). They also suggested that such cooling is largely compensated for by the inclusion of a prognostic skin temperature, since solar heating in the daytime overwhelms cooling in the nighttime.

b. Overview of the selected schemes

Both the SAS and RAS schemes are based on the closure assumption of Arakawa and Schubert (1974), that is, the convective clouds stabilize the environment as fast as the convective processes destabilize it. The original Arakawa-Schubert scheme has been simplified by Grell (1993) with a single cumulus updraft/downdraft couplet within a single grid cell, the resulting scheme being termed the SAS scheme after further modifications at National Center for Environmental Prediction (NCEP) (Pan and Wu, 1995; Hong and Pan, 1998; Park and Hong, 2007). The main differences between the SAS and RAS schemes are two components: the clouds model and the treatment of downdrafts. The SAS scheme allows only one type of cloud, while the RAS scheme allows multiple clouds with different tops. The SAS considers saturated downdrafts on the basis of empirical formulation whereas the RAS does not. These differences result in the models producing different vertical heating and moistening profiles and precipitation patterns. The trigger function for the SAS uses the parcel buoyancy method, whereas the RAS uses the relative humidity near the surface.

The SAS scheme has been operational in the NCEP global forecast system. For short- and medium-range forecasts, the SAS has been recognized to have a good ability to predict tropical precipitation (Kalnay *et al*., 1996). Meanwhile, Kanamitsu *et al*., (2002a) showed that the RAS parameterization scheme outperforms the SAS with regards to the Pacific-North America (PNA) pattern in response to idealized SST forcing over the equatorial Pacific. Park *et al*. (2010) also confirmed the superiority of the RAS scheme over the SAS scheme in reproducing the tropical precipitation and ISO signals.

The CCM scheme (Zhang and McFarlane, 1995) is based on a plume ensemble approach in which it is assumed that an ensemble of convective-scale updrafts and their associated downdrafts may exist when the atmosphere is conditionally unstable in the lower troposphere. The updraft ensemble, composed of plumes rooted in the planetary boundary layer, can penetrate into the upper troposphere until they reach their neutral buoyancy levels. Convection occurs only in the presence of convective available potential energy (CAPE), which is subsequently eliminated due to convection at an exponential rate using a specified adjustment time scale. Zhang and McFarlane (1995) showed that the CCM scheme significantly improves the precipitation, surface evaporation, and surface wind stress in the tropical convective regimes, particularly in the western Pacific warm pool, compared with the previous version, i.e., CCM2. The CCM scheme is further revised by Zhang and Mu (2005), but we employ the original version in this study.

The KF2 scheme (Kain, 2004) is an updated version of the original KF scheme (Kain and Fritsch, 1990). In the KF2 scheme, the closure is based on the CAPE for an entraining parcel, which provides reasonable rainfall rates for a broad range of convective environments. In addition, the updraft algorithm has also been modified with a specified minimum entrainment rate and formulations to permit variability in the cloud radius and cloud-depth threshold for deep (precipitating) convection. The KF2 scheme has been widely used in mesoscal models (e.g., WRF model), successfully applied to mesoscale studies (e.g., Ridout *et al*., 2005), and has been incorporated into real-time forecasts using the WRF (e.g., Byun *et al*., 2011). However, the KF2 scheme has not been applied to GCM studies in the past.

c. Experimental design

A total of four experiments, namely the SAS, RAS, KF2, and CCM experiments are conducted using the SAS, RAS, KF2, and CCM CPS schemes. The ENS experiment is simple ensemble mean of the results from the four CPS experiments.

All simulations are conducted for the eight extended boreal summers (May-June-July-August-September, MJJAS) from 1997 to 2004, as in Park *et al*. (2010). Previous studies have showed that a 5-month period is sufficient to evaluate the characteristics of wave propagation and intensity of the ISO simulation due to different CP schemes (Park *et al*., 2010, Weaver *et al*., 2011). The ocean initial conditions were obtained from the Global Ocean Data Assimilation System (GODAS), which was made operational at NCEP since September 2003. The atmospheric initial conditions were derived from NCEP / Department of Energy (DOE) Reanalysis II (RA2) data (Kanamitsu *et al*., 2002b). As a surface boundary initial condition, observed SST data with a resolution of 1 degree were used (Reynolds and Smith, 1994).

Simulated climatology, including precipitation, large-scale features, and SST, is evaluated against observed monthly and daily precipitation and the observed large-scale fields, which are obtained from the Climate Prediction Center (CPC) Merged Analysis Monthly precipitation (CMAP) data (Xie and Arkin, 1997), the Global Precipitation Climatology Project (GPCP) Satellite-Derived GOES Precipitation Index (GPI) daily Rainfall Estimates products (Huffman *et al*., 2001), RA2 data, and Optimally Interpolated SST (OISST) data.

3. Results

A standardized set of diagnostics developed by the US Climate Variability and Predictability (CLIVAR) MJO Working Group is utilized. Detailed information regarding the diagnostics is available in Waliser *et al*. (2009). Following Park *et al*. (2010), the period of analysis in this study is 5 months (MJJAS).

a. Seasonal mean climatology

The observed rainfall is concentrated in three major areas (Fig. 1a): the Asian monsoon region, the western North Pacific monsoon region, and the inter-tropical convergence zone (ITCZ). The monsoonal precipitation associated with the Asian summer monsoon occurs mainly over the Indian Ocean, where it is directly connected with the Somali jet across the Indian subcontinent. The western North Pacific monsoon is related to the Indonesian branch of the Walker circulation over the warm pool region and produces enhanced tropical precipitation. The observed equatorial rainfall along the ITCZ over the Pacific is associated with the low-level easterly convergence zone.

All experiments reproduced the above-observed features fairly well, with the correlation coefficients greater than 0.8. The SAS experiment reproduces tropical precipitation over the ITCZ, the Pacific, and the Atlantic Ocean (Fig. 1b). However, there are discernible defects, including excessive rainfall in the trade wind region north of the equator. This excessive rainfall is largely corrected for by the RAS scheme (Fig. 1c); however, the RAS run underestimates the amount of precipitation over the Indian Ocean and equatorial eastern Pacific Ocean. Results from the KF2 experiment show similar patterns to those from the SAS experiment, but with an improved reflection of the ITCZ over the central and eastern Pacific (Fig. 1d). The pattern correlation coefficient from the KF2 experiment is 0.87, which is the highest of all the experiments. The experiment using the CCM scheme shows exaggerated precipitation over the Indian Ocean, northwest Pacific Ocean, and equatorial eastern Pacific Ocean (Fig. 1e). The ENS experiment underestimated tropical precipitation in most tropical regions, especially over the western Pacific (Fig. 1f).

Both model results suggest that high mean precipitation (> 11 mm day^{-1}) in the western Pacific is associated with the eastward extension of the westerly zonal wind into that basin (e.g., Inness *et al*., 2003; Sperber *et al*., 2005). The air-sea coupled intraseasonal interaction mechanism for the MJO, proposed by Flatau *et al.* (1997), requires that the low-level winds should be westerly for the coupling between convection and SST to maintain the MJO (Kim *et al*., 1999). Over the tropical western Pacific Ocean, the mean state of 850-hPa zonal wind has been shown to be indicative of the ability of a model to represent ISO convection over this region. Of the experiments analyzed herein, only the ENS experiment does not demonstrate this relationship due to the serious underestimation of precipitation, although the low-level winds over the western Pacific Ocean are similar to what was observed.

The SST bias, defined as modeled SST minus observed SST, is presented in Fig. 2. All the experiments show that cold biases prevail over the northwest Pacific and Indian Oceans.

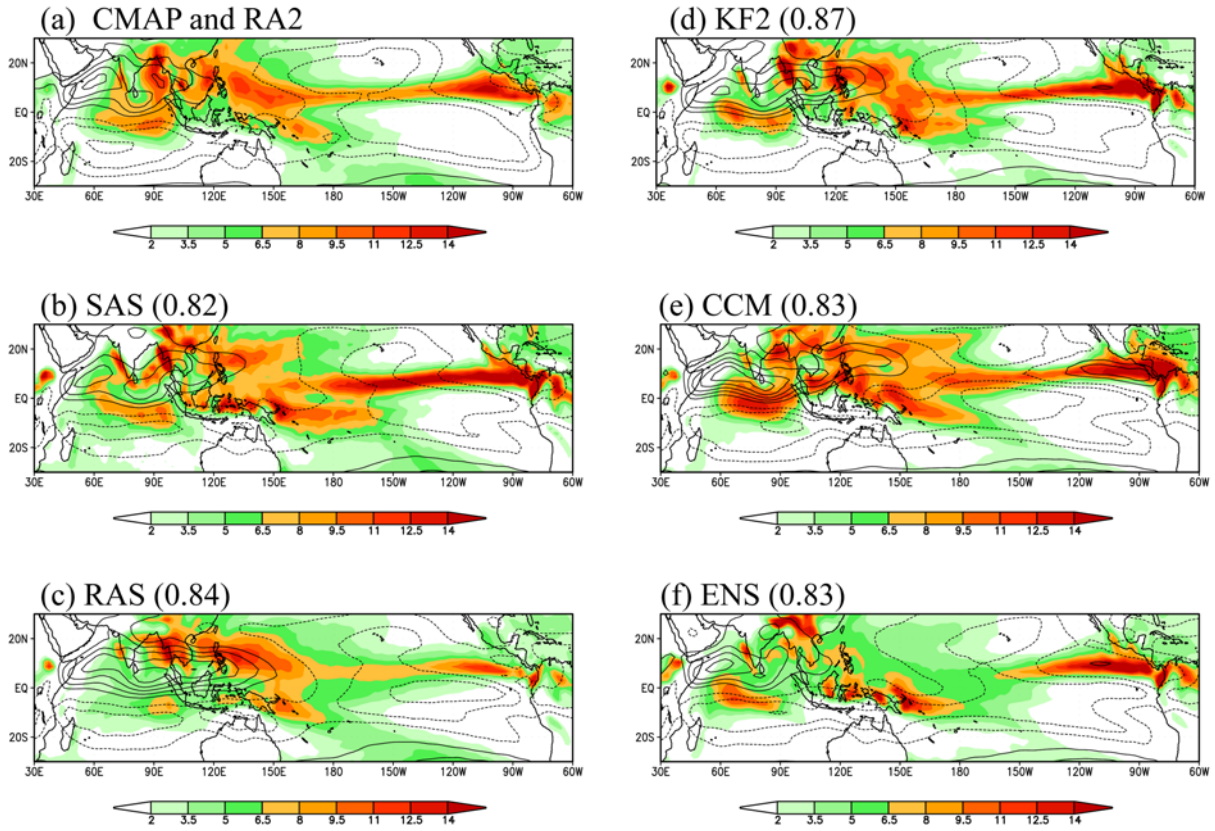

Fig. 1. May-September (1997-2004) mean precipitation (mm day^{-1}) (shaded) and 850-hPa zonal wind (m s^{-1}) (contoured) of (a) CMAP/RA2, (b) SAS, (c) RAS, (d) KF2, (e) CCM, and (f) ENS experiments. The values in parentheses indicate the correlation coefficients between the CMAP and simulated precipitation.

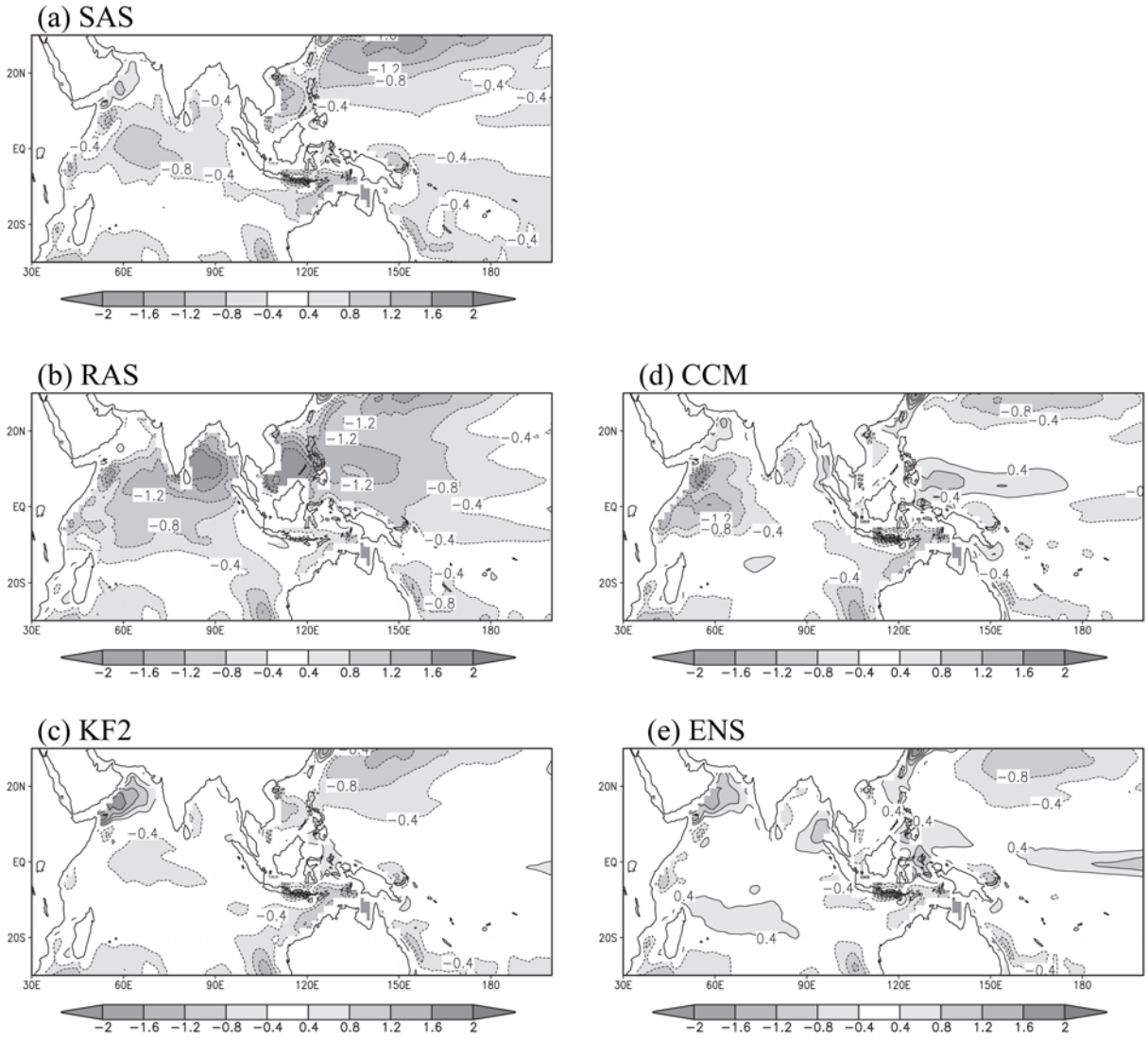

Fig. 2. May-September (1997-2004) mean SST biases (°C) for (a) SAS, (b) RAS, (c) KF2, (d) CCM, and (e) ENS experiments.

The magnitude of biases is largest for the RAS, SAS, KF2, and CCM runs, in that order. The cold bias over the tropics may be due to a stronger upwelling, whereas cooling over the subtropical oceans is attributable to the reduced solar heating by clouds (Seo and Wang, 2010). The significant cold bias in the RAS experiment may be due to a strong upwelling, which is driven by the easterly bias in that region. The suppressed convection due to the cold surface leads to the aggravation of easterly bias through wind-SST feedback. In response to increasing (decreasing) low-level wind speed, evaporation is increased (decreased). Increasing (decreasing) evaporation results in more (less) SST cooling, which in turn further increases (decreases) the low-level wind speed (Wang *et al*., 1999).

b. Intraseasonal oscillation

To demonstrate how the magnitude and geographical distribution of intraseasonal variability are simulated, maps of the 20-100-day filtered variances of precipitation are shown in Fig. 3. In observation, the precipitation variance maximum is located in the eastern Indian Ocean and western Pacific (Fig. 3a). The SAS (Fig. 3b) and KF2 (Fig. 3d) experiments reproduce this pattern fairly well, albeit somewhat exaggerated in terms of magnitude over the Indian Ocean, southwest Pacific, ITCZ, and equatorial eastern Pacific Ocean. Conversely, the RAS run (Fig. 3c) exhibits weakened variance over the tropical oceans that appears to be associated with cold SST bias (cf. Fig. 2b). Intraseasonal variability from the CCM and ENS experiments is too weak (Figs. 3e and 3f). These results seem to be associated with the mesoscale characteristics as seen in previous literature (Kang and Hong, 2008). Kang and Hong (2008) found that in regional climate simulation for a spectral regime larger than about 450 km, the experiments with RAS and CCM schemes do not provide any additional large-scale information over the SAS and KF2 schemes.

Equatorial wavenumber-frequency spectra (Hayashi, 1979)

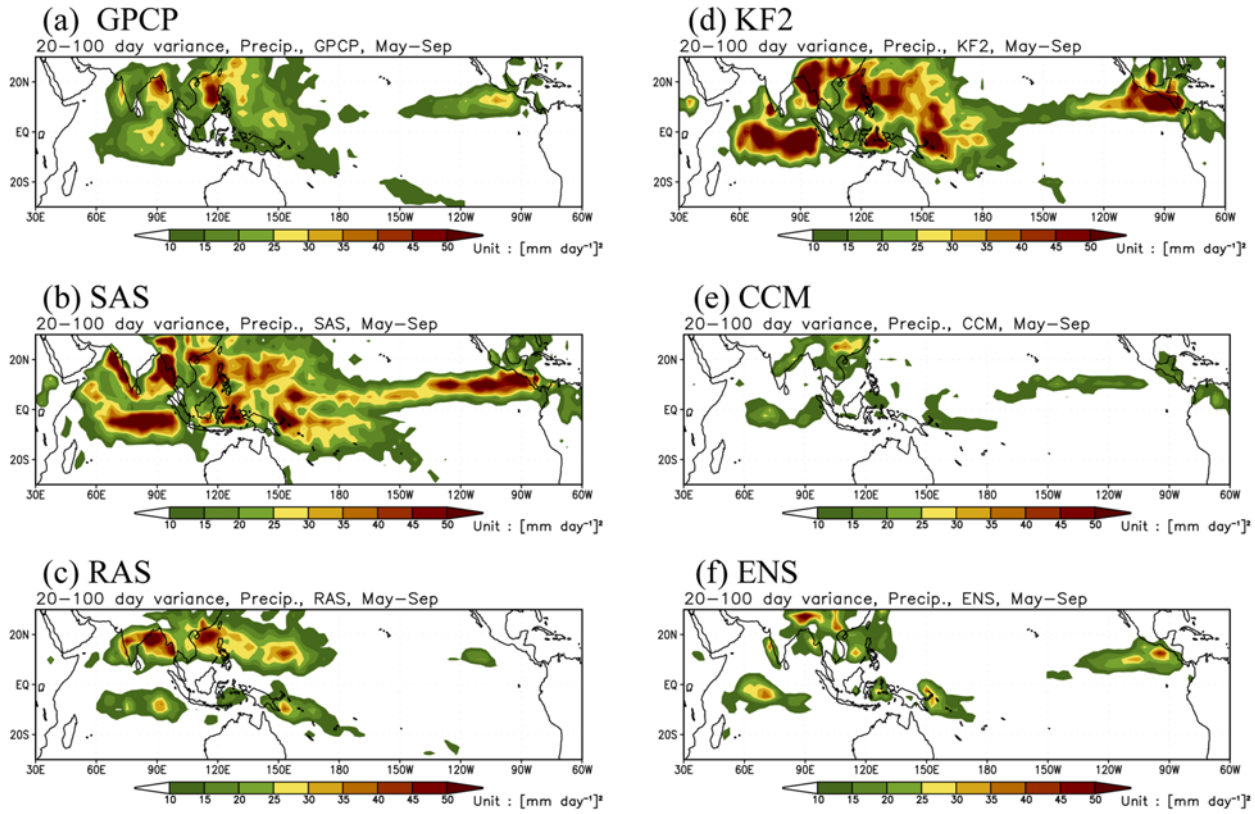

Fig. 3. The 20-100-day precipitation variance (mm^2 day^{-2}) averaged for 8 years from 1997 to 2004. (a) GPCP observation, (b) SAS, (c) RAS, (d) KF2, (e) CCM, and (f) ENS experiment.

for the 850-hPa zonal wind to the isolation of the characteristic spatial and temporal scales on which variability is organized are shown in Fig. 4. The zonal wind was chosen for the analysis of the ISO signal because it is important to the ISO surface energy budget, with implications for air-sea interactions and wind-induced flux forcing of convection (e.g., Hendon, 2000; Inness *et al*., 2003; Bellon *et al*., 2008). The spectra was computed by Fourier transforming 180-day segments centered on the boreal summer, forming power, and then averaging over eight years of data (1997-2004). The resulting bandwidth is $(180\ days)^{-1}$. By definition, eastward propagation is represented by positive frequency and positive wavenumber, whereas westward propagation is represented by either the wavenumber or the frequency being negative. If standing oscillations are present, they will project as equal amounts of power in eastward and westward directions.

Consistent with the results of previous studies (Lawrence and Webster, 2002; Wheeler and Hendon, 2004; Zhang *et al*., 2006; Kim *et al*., 2009), the dominant spatial scale of the 850-hPa zonal wind in observations is zonal wavenumber 1 for periods of 30-80 days (Fig. 4a). The eastward power is about four times that of westward power at intraseasonal frequencies and spatial scales characteristic of the ISO. All experiments reproduce a spectrum with wavenumber 1, which is similar to the observed spectra. For most experiments, eastward propagating power tends to be concentrated at low frequency (period > 80 days). The RAS experiment reveals a spectrum with a frequency of 30-80 days, similar to that from RA2, but with the exaggerated magnitude (Fig. 4c). Meanwhile, the wavenumber spectra in the eastward and westward directions for the SAS and KF2 experiments are similar to each other (Figs. 4b and 4d). The spectra in the westward direction are underestimated in the CCM experiment (Fig. 4e). The ensemble does not provide a distinct advantage over other experiments (Fig. 4f).

To assess whether the extracted ISO modes are physically meaningful and distinct from a red noise process, the power spectra of an unfiltered 850-hPa zonal wind was calculated over the Indian Ocean (68.75°E-96.25°E, 3.75°N-21.25°N) from the RA2 and model simulations (Fig. 5). In RA2, the spectral power that is statistically significant at the 95% confidence level, relative to a red noise process, is concentrated near a period of 50 days and related to the ISO modes (Fig. 5a). The SAS experiment also shows the power to be statistically significant near a period of 50 days, although it is concentrated at low frequencies (> 80 day) (Fig. 5b). In the RAS experiment, the period related to the ISO signal is near the ISO time scale (about 50 days); however, the power is exaggerated (Fig. 5c). The KF2 has the largest variance at a period of 40 days and dominant peaks at periods less than 30 days (Fig. 5d). The CCM and ENS experiments are dominated by excessive power at low frequencies (Figs. 5e and 5f).

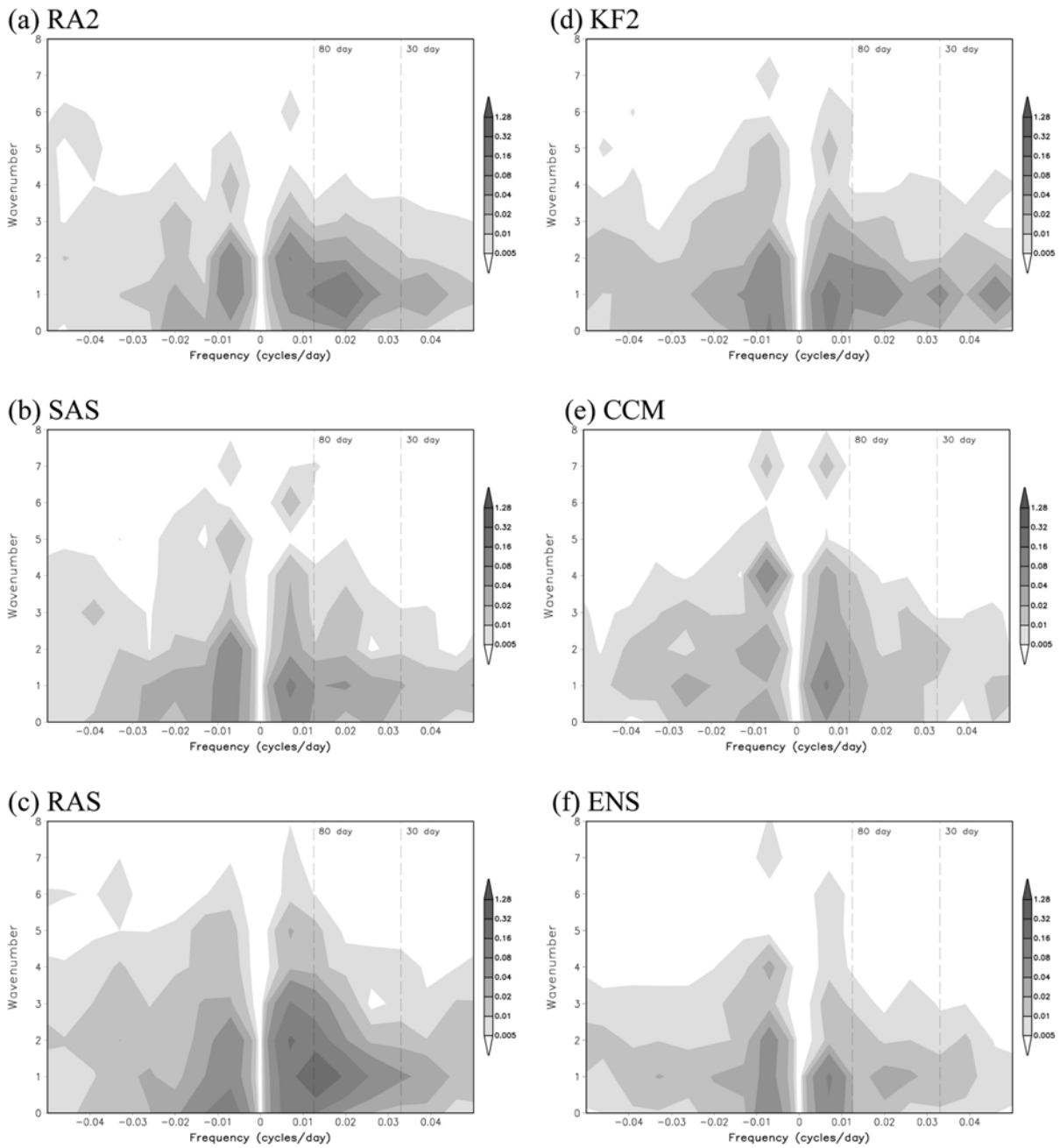

Fig. 4. May-September wavenumber-frequency spectra of 10°N-10°S averaged 850-hPa zonal wind (m^2 s^{-2}) for the (a) RA2, (b) SAS, (c) RAS, (d) KF2, (e) CCM, and (f) ENS experiments. Individual May-September spectra were calculated for each year and then averaged over all years of data. Only the climatological seasonal cycle and time mean for each May-September segment were removed before calculation of the spectra. The bandwidth is $(180 \text{ days})^{-1}$.

Recently, some studies have used Combined Empirical Orthogonal Function (CEOF) to analyze the ISO signal (e.g., Kim *et al*., 2009; Park *et al*., 2010; Seo and Wang, 2010). We use the CEOF diagnostics developed by CLIVAR MJO Working Group in which outgoing longwave radiation (OLR), 850-hPa zonal wind, and 200-hPa zonal wind are used to extract the MJO modes (Waliser *et al*., 2009). This multivariate approach isolates the convective and baroclinic zonal wind signature of the MJO. Wheeler and Hendon (2004) used unfiltered input data to the CEOF analysis to develop a real-time MJO diagnostic for their experimental MJO system, whereas we use 20- to 100-day bandpass-filtered data to isolate the ISO modes, which is consistent with Kim *et al*. (2009).

The first two CEOFs from observations and the experiments are shown in Fig. 6. In observations, the second mode, seen in the upper panel of Fig. 6a, captures the enhanced convective activity over the eastern Indian Ocean and Maritime Continent. The first mode captures the enhanced convection over the

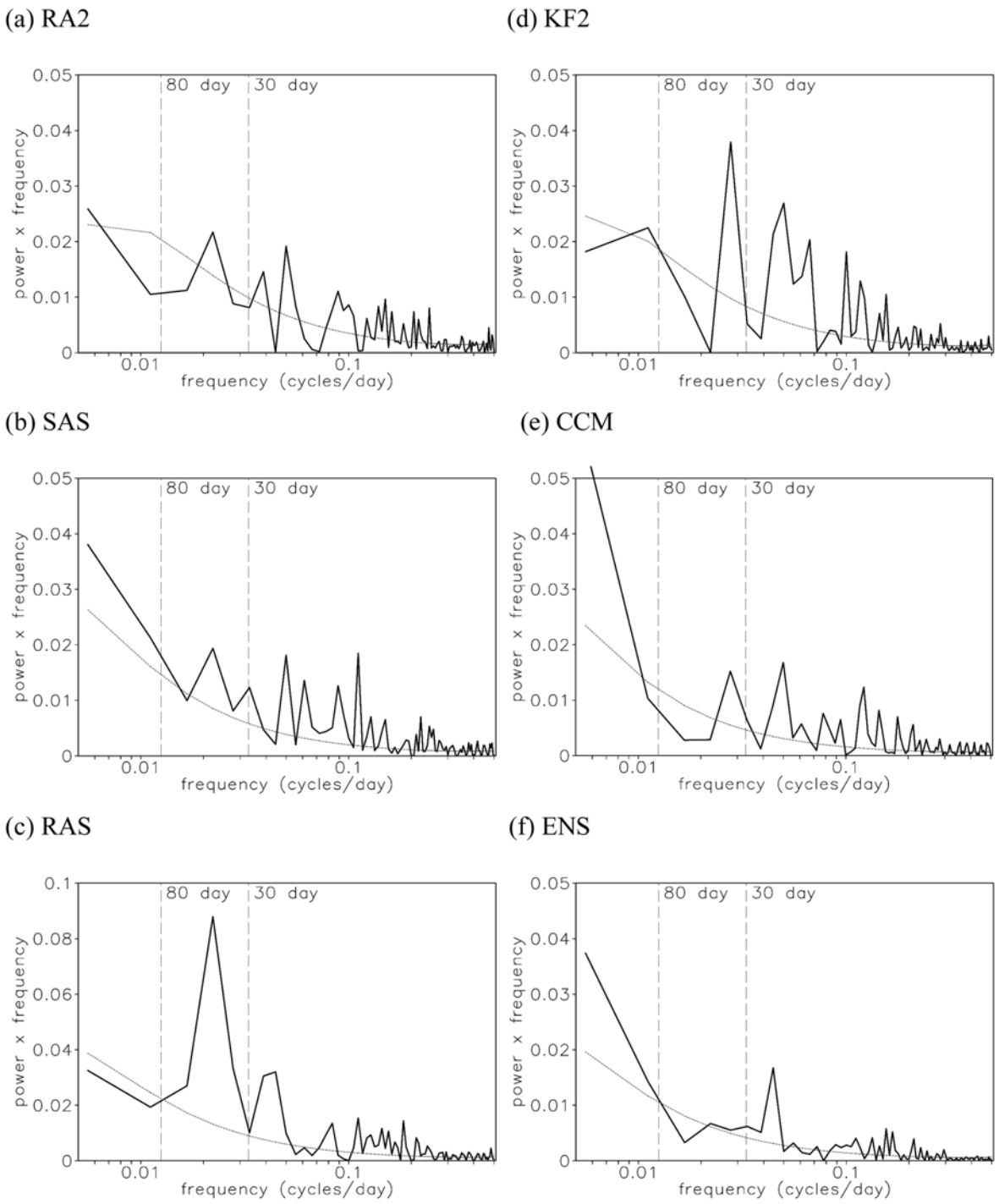

Fig. 5. The power spectra of daily 850-hPa zonal wind anomalies for the boreal summers from 1997 to 2004. 850-hPa zonal winds are area averaged over the domain of 3.75°N~21.25°N and 68.75°E~96.25°E. Dotted lines show the upper 95% confidence limits of the red noise spectrum.

western/central Pacific Ocean and the suppressed convection over the Indian Ocean, as shown in the lower panel of Fig. 6a. As seen in these figures, the upper (black dashed line) and lower (black solid line) troposphere zonal winds are out of phase, indicating a baroclinic structure of the ISO. Additionally, the zonal wind maxima are displaced relative to the convection signal, with low-level easterlies tending to lead the convective maximum.

In the SAS experiment, the enhanced convection over the Indian Ocean is captured in the first mode, but convection over the central Pacific Ocean is not captured by the second mode (Fig. 6b). In addition, the amplitude of OLR is very small and its phase is unstable compared to observations. In the RAS experiment, the upper (black dashed line) and lower (black solid

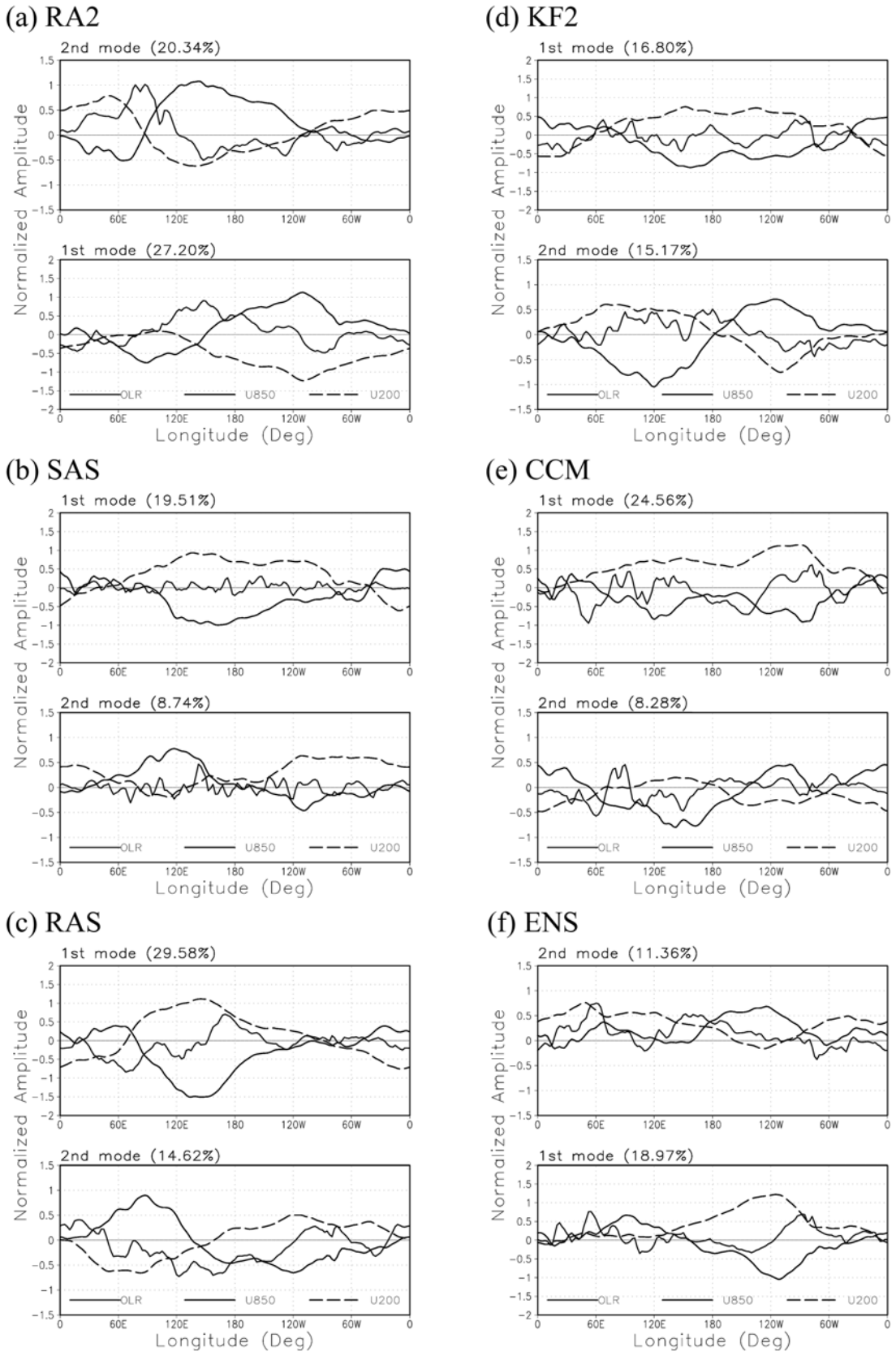

Fig. 6. First two CEOF modes of 20-100-day 15S-15N averaged 850-hPa and 200-hPa zonal wind and OLR for the (a) RA2, (b) SAS, (c) RAS, (d) KF2, (e) CCM, and (f) ENS experiments. Sign and location (upper or lower) of each mode are arbitrarily adjusted to be similar to observation. The mode having the largest percentage variance explained is the first mode.

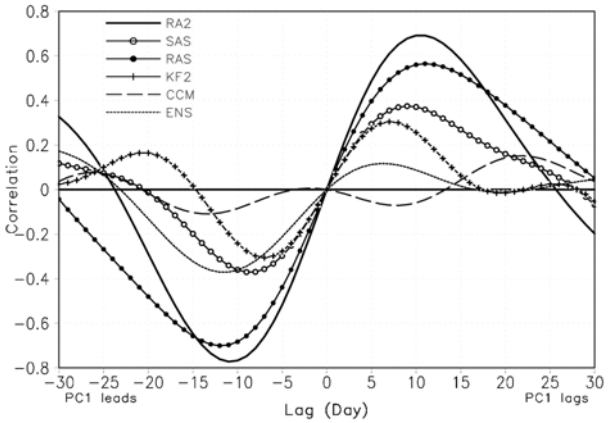

Fig. 7. Lag correlation between the two PCs. A positive lag means that PC2 leads PC1 except for RA2 and ENS experiments, in which PC1 leads PC2.

line) troposphere zonal winds are out of phase with each other, demonstrating the baroclinic structure of the ISO, although the amplitude of OLR is not captured amplitude related to the ISO (Fig. 6c). The first and second modes explain more than 44% of the filtered variance, similar to the observation data. In KF2, although the upper and lower troposphere zonal winds are out of phase with each other, the filtered variance is too weak (about 31%) to demonstrate the baroclinic structure of the ISO (Fig. 6d). Results from the CCM and ENS runs do not capture the eastward propagating ISO and show unstable phases for all variables (Figs. 6e and 6f).

A plot of the lag correlation between the two Principal Components (PCs) is shown in Fig. 7, where positive lag means that PC2 leads PC1. Since the two PCs correspond to active convection in the Indian Ocean and in the Maritime Continents/western Pacific Ocean, the point of greatest lag correlation approximates the propagation time from the Indian Ocean to the western Pacific, or a quarter of the oscillation period. The figure shows the propagation time to be about 10 days in both the observation and RAS experiment. However, the propagation times from the other experiments are shorter than the observed time. Relative to the observations, the RAS experiment gives a similar correlation value in addition to the similar propagation speed. In contrast, results from other experiments produce smaller correlations and shorter propagation times compared to the observation data, and thus a less robust ISO signal.

These results suggest that the removal of a cold SST bias cannot always guarantee eastward propagation across the Maritime Continent to the dateline as seen in the observations. The RAS run shows that even if a cold bias exists over the tropical western Pacific, the eastward propagation is greatly enhanced due to eastward wind bias.

c. Discussion

To understand the physical processes causing this sensitivity, the vertical profiles of differences in temperature and relative humidity between the simulated results and RA2 data are plotted in Fig. 8. The analysis region is the Indian Ocean (68.75°E-96.25°E, 3.75°N-21.25°N), as seen in Fig. 5. It was found that the characteristics of the analyzed profiles are not sensitive to the selected domain in the Indian Ocean. Overall, the vertical structures of the bias patterns are similar for all

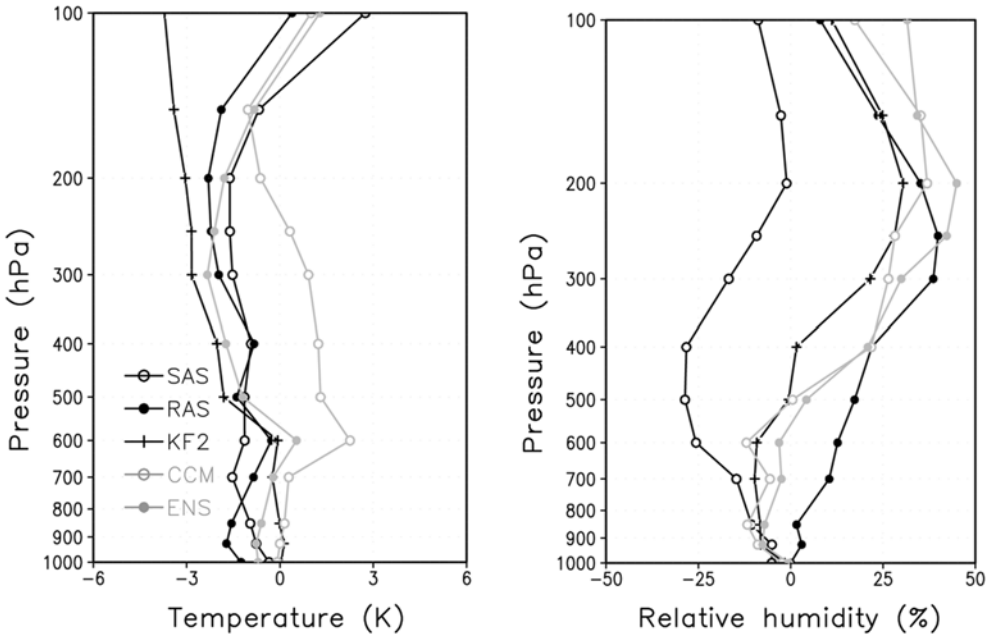

Fig. 8. Vertical profiles of difference in temperature (K) and relative humidity (%) averaged over the domain of 3.75°N~21.25°N and 68.75°E~96.25°E between RA2 data and each experiment.

runs, although their magnitudes differ. For temperature (Fig. 8a), a warming is distinct below 200 hPa in the CCM experiment, whereas cold biases are observed in the other experiments. In particular, the bias patterns from the SAS and RAS runs are very similar, which is partly due to same closure as Arakawa and Schubert (1974). Warm biases in the CCM experiment can be attributed to convection that is vigorous relative to that from the other experiments (cf., Fig. 1).

Regarding moisture bias (Fig. 8b), the SAS run shows maximum dryness to occur at 500 hPa, whereas moistening appears in the upper troposphere in the other experiments. Compared to the differences in temperature, the diversity of moisture biases is relatively large. For example, the SAS and RAS runs exhibit distinct drying and moistening, respectively, whereas both experiments reveal similar temperature profiles that are associated with lower and greater amounts of precipitation in the RAS and SAS runs, respectively (Fig. 1).

Relative humidity is regarded to be an important variable for amplification of the ISO through the creation of a time lag between condensational heating and large-scale convergence (Fu and Wang, 2009). The formation of stratiform rainfall in the model largely depends on the relative humidity (Roeckner *et al*., 1996). The drier mid-troposphere in the SAS experiment suppresses the formation of stratiform rainfall and the associated moisture-stratiform instability (Kuang, 2008; Fu and Wang, 2009; Seo and Wang, 2010). Fu and Wang (2009) argued that maintaining an adequate partitioning between stratiform and convective rainfall is a critical factor in sustaining the MJO.

Figure 9 compares the horizontal distribution of convective and stratiform precipitation. In GCM experiments, total precipitation can be divided between stratiform and convective precipitation. Stratiform precipitation is obtained by grid-resolvable processes, whereas convective precipitation is produced by the parameterized sub-grid scale processes from a CPS. All experiments show that convective precipitation is dominant because the model resolution is relatively coarse (cf. Fig. 1 and Fig. 9). The amount of stratiform precipitation over the tropics is largest in the RAS, CCM, KF2, and SAS experiments, in that order. The most of tropical precipitation from the SAS experiment is due to the CPS scheme, whereas precipitation over the Indian Ocean in the RAS experiment is largely due to the stratiform processes (cf., Figs. 9a and 9b). It is noted that the CCM scheme simulates much of the stratiform precipitation over the central Pacific (Fig. 9d).

Higher humidity leads to easier penetration of convective clouds through the entire column of the troposphere without significant dilution by entrainment of dry air. The RAS scheme considers cumulus ensembles with different cloud tops and so allows convective detrainment of moist air to the environment at the various levels. This detrainment enables an increase in the relative humidity of the environment in the middle-upper troposphere, which brings about vigorous large-scale condensation and stratiform rainfall. Conversely, the SAS scheme considers one deep cloud with detrainment at the cloud tops only, which leads to less moistening in the environment and

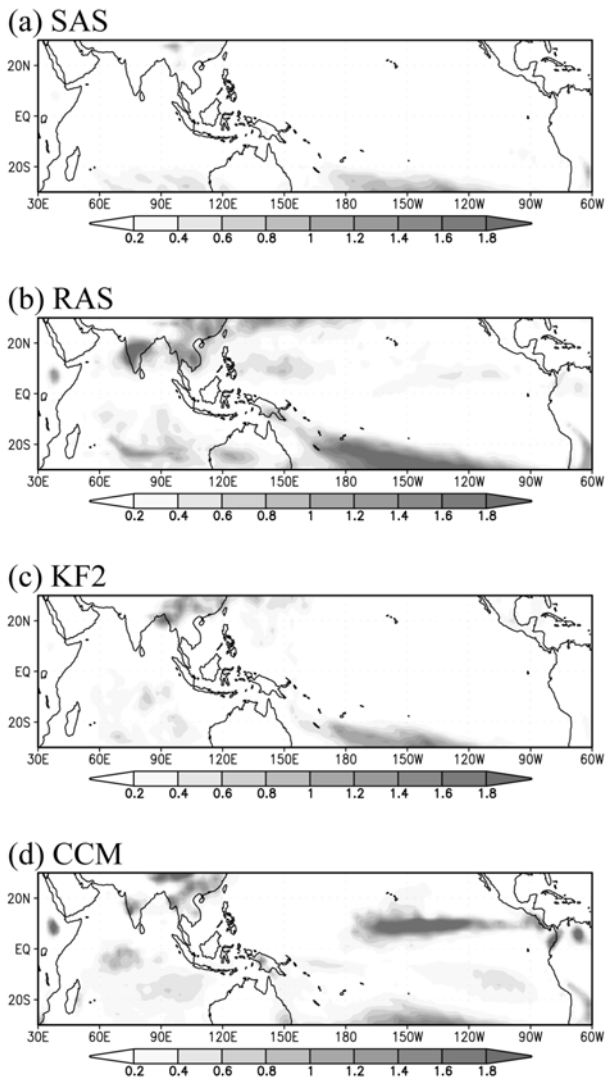

Fig. 9. May-September (1997-2004) averaged stratiform precipitation (mm day^{-1}) of (a) SAS, (b) RAS, (c) KF2, and (d) CCM experiments.

therefore lower stratiform rainfall than is seen in the RAS scheme. Dryness in the CCM and KF2 experiments also show smaller amounts of stratiform precipitation than the RAS run. That is, the differences in stratiform precipitation between the runs result in the different detrainment of water vapor from convective clouds in the middle and upper troposphere, which ultimately affects the development and propagation of the ISO. These finding are consistent with other studies (e.g., Seo and Wang, 2010).

4. Concluding remarks

In this study, we investigate the sensitivity of tropical intraseasonal oscillations in a coupled climate model to four CPSs, namely the simplified Arakawa-Schubert (SAS), relaxation Arakawa-Schubert (RAS), new Kain-Fritsch (KF2), and National Center for Atmospheric Research (NCAR) Climate Model version 3 (CCM) schemes. The ensemble mean of the

results from the four experiments is also examined. The characteristics of wave propagation and the intensity of the ISO simulated by the model, together with the mean climatology, are investigated for extended boreal summers from 1997 to 2004.

The simulated tropical precipitation climatology shows that all experiments capture the pattern fairly well, as evidenced by the pattern correlation coefficients being greater than 0.8. Interestingly, although the KF2 scheme has been widely tested and updated in the mesoscale modeling area, its capability in simulating the tropical climate is relatively good in terms of SST and precipitation. The SAS and KF2 runs exhibit greater precipitation variance than the other experiments, which seems to be associated with the mesoscale characteristics as seen in the previous literature. Analyses of ISO signals in terms of wavenumber-frequency spectra, power spectra of 850-hPa zonal winds, the first two CEOF models of 20-100 day periods over the Indian Ocean, and lag correlation between the two PCs demonstrate that the RAS scheme generally outperforms the other schemes despite overestimating the spectra. The SAS and KF2 schemes show similar patterns in the ISO signals, whereas the CCM scheme fails shows intensity that is too weak.

It has been well known that the physical ensemble approach plays an important role in reducing uncertainties embedded within the parameterization of physical processes in seasonal forecasts (e.g., LaRow *et al*., 2005). However, in this study, the ensemble mean of results from the four experiments does not reveal any benefit in reproducing the observed precipitation climatology and ISO signals, apparently because the individual experiments reproduce the observed features fairly well and do not enhance undesirable noises. Further, the overall quality of simulations is better than that achieved by Park *et al*. (2010). In addition to the inclusion of air-sea interaction in this study, the revised physics package of the GRIMs (Hong *et al*., 2013) over that used in Park *et al*. (2010) is another factor.

Maintaining an adequate partitioning between stratiform and convective rainfall is a critical factor in sustaining the ISO modes. The relationships between stratiform precipitation and ISO in each experiment were also investigated. The amount of corresponding stratiform precipitation over the Indian Ocean in the RAS run is much larger than that seen in the other experiments. Higher humidity is known to ease penetration of convective clouds. The inclusion of cumulus ensembles with different cloud tops in the RAS scheme enables an increase in relative humidity in the middle-upper troposphere and stronger large-scale condensation and stratiform precipitation, which ultimately affects the development and propagation of the ISO. Consequently, this study suggests that improvement of the prediction of ISO in GCMs requires not only an understanding of the mechanism driving ISO development and propagation, but also the incorporation of sophisticated cloud microphysics for realistic stratiform precipitation.

Despite increasing our understanding of the role of the CPS, this study does not definitively show accurate ISO simulation to guarantee improved seasonal predictability of boreal summer precipitation, which is counter to the conclusion of Park *et al*. (2010). A positive feedback between easterly wind and cold SST biases over the tropics that appears in the case of the RAS scheme results in suppressed deep convection over the Indian Ocean that aggravates the seasonal mean precipitation. However, the moisture remaining in the atmosphere enhances the stratiform type precipitation, and together with the characteristic of the RAS scheme having multiple cloud tops, serves as the major cause for success in reproducing the ISO signals, which is in agreement with the results of Seo and Wang (2010).

Our study implies that the appropriate partitioning of deep convection due to CPS and stratiform precipitation due to the microphysics scheme should be taken into account when developing or revising physics algorithms in coupled GCMs. Also, further evaluation of CPSs at higher resolutions for a long-term period is needed.

Acknowledgements. We would like to thank the anonymous reviewers for their helpful and constructive comments and suggestions. This work was supported by the Basic Science Research Program through the National Research Foundation of Korea (NRF) funded by the Ministry of Education, Science and Technology (2012-0000158) and also funded by the Korea Meteorological Administration Research and Development Program under Grant CATER 2012-3084. The authors would like to acknowledge the support from the KISTI supercomputing center through the strategic support program for supercomputing application research [No. KSC-2011-C3-11].

Edited by: Tianjun Zhou

REFERENCES

Arakawa, A., and W. H. Schubert, 1974: Interaction of a cumulus cloud ensemble with the large scale environment. Part I: *J. Atmos. Sci.*, **31**, 674-701.

Bellon, B., A. Sobel, and J. P. Vialard, 2008: Ocean-atmosphere coupling in the monsoon intraseasonal oscillation: A simple model study. *J. Climate*, **21**, 5254-5270.

Bessafi, M., and M. C. Wheeler, 2006: Modulation of South Indian Ocean tropical cyclones by the Madden-Julian oscillation and convectively coupled equatorial waves. *Mon. Wea. Rev.*, **134**, 638-656.

Byun, U.-Y., S.-Y. Hong, H. Shin, J.-W. Lee, J.-I. Song, S.-J. Hahm, J.-K. Kim, H.-W. Kim, and J.-S. Kim, 2011: WRF-based Short-Range Forecast System of the Korea Air Force: Verification of prediction skill in 2009 summer. *Atmosphere*, **21(2)**, 197-208. (in Korean with English abstract).

Chao, W. C. and L. Deng, 1998: Tropical intraseasonal oscillation, super cloud clusters, and cumulus convection schemes. Part II: 3D aqua-planet simulation. *J. Atmos. Sci.*, **54**, 2429-2440.

Chen, S. S., R. A. Houze, and B. E. Mapes, 1996: Multiscale variability of deep convection in relation to large-scale circulation in TOGA COARE. *J. Atmos. Sci.*, **53**, 1380-1409.

Cheong, H.-B., 2006: A dynamical core with double fourier series: comparison with the spherical harmonics method. *Mon. Wea. Rev.*, **134**, 1299-1315.

Chou, M.-D., and M. J. Suarez, 1999: A solar radiation parameterization for atmospheric studies. Vol. 15, NASA/TM-1999-104606, 38 pp.

_____, and K.-T. Lee, 2005: A parameterization of the effective layer emission for infrared radiation calculation. *J. Atmos. Sci.*, **62,** 531-541.

_____, _____, S.-C. Tsay, and Q. Fu, 1999: Parameterization for cloud longwave scattering for use in atmospheric models. *J. Climate*, **12**, 159-169.

Chun, H.-Y., and J.-J. Baik, 1998: Momentum flux by thermally induced internal gravity waves and its approximation for large-scale models. *J. Atmos. Sci.*, **55**, 3299-3310.

Frank, W. M., and P. E. Roundy, 2006: The role of tropical waves in tropical cyclogenesis. *Mon. Wea. Rev.*, **134**, 2397-2417.

Flatau, M., P. Flatau, P. Phoebus, and P. Niiler, 1997: The feedback between equatorial convection and local radiative and evaporative processes: The implications for intraseasonal oscillations. *J. Atmos. Sci.*, **54**, 2373-2386.

Fu, X., B. Yang, G. Bao, and B. Wang, 2008: Sea surface temperature feedback extends the predictability of tropical intraseasonal oscillation. *Mon. Wea. Rev.*, **136**, 577-597.

_____, and B. Wang, 2009: Critical roles of the stratiform rainfall in sustaining the Madden-Julian oscillation: GCM experiments. *J. Climate*, **22**, 3939-3959.

Grell, G. A., 1993: Prognostic evaluation of assumptions used by cumulus parameterization. *Mon. Wea. Rev.*, **121**, 764-787.

Hayashi, Y., 1979: A generalized method of resolving transient disturbances into standing and traveling waves by space-time spectral analysis. *J. Atmos. Sci.*, **36**, 1017-1029.

Hendon, H. H., 2000: Impact of air-sea coupling on the Madden-Julian oscillation in a general circulation model. *J. Atmos. Sci.*, **57**, 3939-3952.

Hong, S.-Y., and H.-L. Pan, 1998: Convective trigger function for mass flux cumulus parameterization scheme. *Mon. Wea. Rev.*, **126**, 2599-2620.

_____, H.-M. H. Juang, and Q. Zhao, 1998: Implementation of prognostic cloud scheme for a regional spectral model. *Mon. Wea. Rev.*, **126**, 2621-2639.

_____, Y. Noh, and J. Dudhia, 2006: A new vertical diffusion package with an explicit treatment of entrainment processes. *Mon. Wea. Rev.*, **134**, 2318-2341.

_____, _____, and E.-C. Chang, 2012: Spectral nudging sensitivity experiments in a regional climate model. *Asia-Pacific J Atmos Sci*., **48**, 345-355.

_____, and Coauthors, 2013: The Global/Regional Integrated Model system (GRIMs). *Asia-Pacific J. Atmos. Sci*., **49(2)**, 219-243.

Huffman, G. J., R. F. Adler, M. Morrissey, D. T. Bolvin, S. Curtis, R. Joyce, B. McGavock, and J. Susskind, 2001: Global precipitation at one-degree daily resolution from multisatellite observations. *J. Hydrometeor.*, **2**, 36-50.

Inness, P. M., and J. M. Slingo, 2003: Simulation of the Madden-Julian oscillation in a coupled general circulation model. Part I: Comparison with observations and an atmosphere-only GCM. *J. Climate*, **16**, 345-364.

_____, _____, E. Guilyardi, and J. Cole, 2003: Simulation of the Madden-Julian oscillation in a coupled general circulation model. Part II: The role of the basic state. *J. Climate*, **16**, 365-382.

Jeon J.-H., S.-Y. Hong, H.-Y. Chun, and I.-S. Song, 2010: Test of a convectively forced gravity wave drag parameterization in a general circulation model. *Asia-Pacif J. Atmos Sci*., **46**, 1-10.

Jones, C., 2000: Occurrence of extreme precipitation events in California and relationships with the Madden-Julian oscillation. *J. Climate*, **13**, 3576-3587.

Kain, J. S., and J. M. Fritsch, 1990: A one-dimensional entraining/detraining plume model and its application in convective parameterization. *J. Atmos. Sci.*, **33**, 1890-1910.

_____, 2004: The Kain-Fritsch convective parameterization: An update, *J. Appl. Meteorol.*, **43**, 170-181.

Kalnay, E., and Coauthors, 1996: The NCEP/NCAR 40-year reanalysis project, *Bull. Amer. Meteor. Soc.*, **77**, 437-471.

Kanamitsu, M., and Coauthors, 2002a: NCEP Dynamical Seasonal Forecast System 2000. *Bull. Amer. Meteor. Soc.*, **83**, 1019-1037.

_____, W. Ebisuzaki, J. Woollen, S.-K. Yang, J. J. Hnilo, M. Fiorino, and G. L. Potter, 2002b: NCEP-DOE AMIP-II Reanalysis (R-2). *Bull. Amer. Meteor. Soc.*, **83**, 1631-1643.

Kang, H.-S., and S.-Y. Hong, 2008: Sensitivity of the simulated East Asian summer monsoon climatology to four convective parameterization schemes. *J. Geophys. Res.*, **113**, D15119, doi:10.1029/2007JD009692.

Kara, A. B., P. A. Rochford, and H. E. Hurlburt, 2003: Mixed layer depth variability over the global ocean. *J. Geophys. Res.*, **108(C3)**, 3079, doi: 10.1029/2000JC 000736.

Kiladis, G. N., K. H. Straub, and P. T. Haertel, 2005: Zonal and vertical structure of the Madden-Julian oscillation. *J. Atmos. Sci.*, **62**, 2790-2809.

Kim, D., and Coauthors, 2009: Application of MJO simulation diagnostics to climate models. *J. Climate*, **22**, 6413-6436.

Kim, E.-J., and S.-Y. Hong, 2010: Impact of air-sea interaction on East Asian summer monsoon climate in WRF. *J. Geophys. Res.*, **115**, D19118, doi:10.1029/ 2009JD013253.

Kim, Y.-J., and A. Arakawa, 1995: Improvement of orographic gravity wave parameterization using a mesoscale gravity wave model. *J. Atmos. Sci.*, **52**, 1875-1902.

Lawrence, D. M., and P. J. Webster, 2002: The boreal summer intraseasonal oscillation: Relationship between northward and eastward movement of convection. *J. Atmos. Sci.*, **59**, 1593-1606.

Lee, M.-I., I.-S. Kang, and B. E. Mapes, 2003: Impacts of cumulus convection parameterization on aqua-planet AGCM simulations of tropical intraseasonal variability. *J. Meteor. Soc. Japan*, **81**, 963-992.

Lin, J.-L, and Coauthors, 2006: Tropical intraseasonal variability in 14 IPCC AR4 climate models. Part I: Convective signals. *J. Climate*, **19**, 2665-2690.

Madden, R. A., and P. R. Julian, 1971: Detection of a 40-50 day oscillation in the zonal wind in the tropical Pacific. *J. Atmos. Sci.*, **28**, 702-708.

Maloney, E. D., and P. R. Julian, 2001: The sensitivity of intraseasonal variability in the NCAR CCM3 to changes in convective parameterization. *J. Climate*, **14**, 2015-2034.

Mo, K. C., and R. W. Higgins, 1998: Tropical influences on California precipitation. *J. Climate*, **11**, 412-430.

Moorthi, S. and M. J. Suarez, 1992: Relaxed Arakawa-Schubert: a parameterization of moist convection for general circulation models. *Mon. Wea. Rev.*, **120**, 978-1002.

Pacanowski, R. C., and S. M. Griffies, 1998: MOM 3.0 manual. NOAA/ Geophysical Fluid Dynamics Laboratory, Princeton, NJ, 668 pp.

Pan, H.-L., and W.-S. Wu, 1995: Implementing a mass flux convective parameterization package for the NMC medium-range forecast model, in *NMC Office Note 409*, 40 pp., NCEP/EMC, Camp Springs, Md.

Park, H., and S.-Y. Hong, 2007: An evaluation of a mass-flux cumulus parameterization scheme in the KMA Global Forecast System. *J. Meteor. Soc. Japan*, **85**(2), 151-169.

Park, S., S.-Y. Hong, and Y.-H. Byun, 2010: Precipitation in boreal summer simulated by a GCM with two convective parameterization scheme: Implications of the intraseasonal oscillation for dynamic seasonal prediction. *J. Climate*, **23**, 2801-2816.

Reynolds, R. W., and T. M. Smith, 1994: Improved global sea surface temperature analysis using optimum interpolation. *J. Climate*, **7**, 929-948.

Ridout, J. A., Y. Jin, and C.-S. Liou, 2005: A cloud-base quasi-balance onstraint for parameterized convection: Application to the Kain-Fritsch cumulus scheme. *Mon. Wea. Rev.*, **133**, 3315-3334.

Roeckner, E., and Coauthors, 1996: *The atmospheric general circulation model ECHAM-4: Model description and simulation of present-day*

climate. MPI Rep., **218**, 94 pp.

Seo, K.-H., and W. Wang, 2010: The Madden-Julian oscillation simulated in the NCEP climate forecast system model: The importance of stratiform heating. *J. Climate*, **23**, 4770-4793.

Skamarock, W. C., and Coauthors, 2008: *A description of the advanced research WRF version 3*. NCAR Tech. Note NCAR/TN-475+STR, 113 pp.

Sperber, K. R., S. Gualdi, S. Legutke, and V. Gayler, 2005: The Madden-Julian oscillation in ECHAM4 coupled and uncoupled general circulation models. *Climate Dyn.*, **25**, 117-140.

Tian, B. J., D. E. Waliser, and E. J. Fetzer, 2006: Modulation of the diurnal cycle of tropical deep convective clouds by the MJO. *Geophys. Res. Lett.*, **33**, L20704, doi:10.1029/2006GL027752.

Waliser, D. E., and Coauthors, 2009: MJO Simulation Diagnostics. *J. Climate*, **22**, 3006-3030.

Wang, C., R. H. Weisberg, and H. Yang, 1999: Effects of the Wind Speed-Evaporation-SST feedback on the El Nino-Southern Oscillation. *J. Atmos. Sci.*, **56**, 1391-1403.

Wang, W. Q., and M. E. Schlesinger, 1999: The dependence on convection parameterization of the tropical intraseasonal oscillation simulated by the UIUC 11-layer atmospheric GCM. *J. Climate*, **12,** 1423-1457.

Weaver, S. J., W. Wang, M. Chen, and A. Kumar, 2011: Representation of MJO variability in the NCEP Climate Forecast System. *J. Climate*, **24**, 4676?4694.

Wheeler, M. C., and H. H. Hendon, 2004: An all-season real-time multivariate MJO index: Development of an index for monitoring and prediction. *Mon. Wea. Rev.*, **132**, 1917-1932.

Xie, P., and P. A. Arkin, 1997: Global precipitation: A 17-year monthly analysis based on gauge observations, satellite estimates, and numerical model outputs. *Bull. Amer. Meteor. Soc.*, **78**, 2539-2558.

Zhang, C., M. Dong, S. Gualdi, H. H. Hendon, E. D. Maloney, A. Marshall, K. R. Sperber, and W. Q. Wang, 2006: Simulations of the Madden-Julian oscillation in four pairs of coupled and uncoupled global models. *Climate Dyn.*, **27**, 573-592.

Zhang, G. J., and N. A. McFarlane, 1995: Sensitivity of climate simulations to the parameterization of cumulus convection in the Canadian climate centre general circulation model. *Atmos.-Ocean*, **33**, 407-446.

_____, and M. Mu, 2005: Simulation of the Madden-Julian oscillation in the NCAR CCM3 using a revised Zhang-McFarlane convection parameterization scheme, *J. Climate*, **18**, 4046-4064.